Ninth International Conference on
THIN-WALLED STRUCTURES – ICTWS2023
Sydney, Australia, Nov 29 – Dec 1, 2023

BUCKLING ANALYSIS OF BUILT-UP COLD-FORMED STEEL MEMBERS USING THE REPRODUCING KERNEL PARTICLE FINITE STRIP METHOD

Mani Khezri*

* School of Civil Engineering, The University of Sydney
e-mails: mani.khezri@sydney.edu.au

Keywords: Reproducing Kernel Particle Method; Finite Strip Method; Buckling analysis; Built-up Cold-Formed Steel, Discrete Fasteners.

Abstract. *In this paper, the application of the Reproducing Kernel Particle Finite Strip Method (RKP-FSM) to the stability analysis of cold-formed steel built-up sections is explored. The representation of the employed fasteners is achieved through the constraint of degrees of freedom using equations, and the impact of connection elements is incorporated into the overall stiffness matrix of the built-up sections. This method enables the modelling of discrete fasteners located at arbitrary positions within the framework of RKP-FSM. To validate the efficacy of the proposed numerical technique, comparisons are made with finite element solutions across a range of numerical examples, affirming its accuracy and versatility. An array of built-up sections, spanning typical and intricate configurations with varying fastener arrangements and end boundary conditions, are analysed to evaluate the influence of fastener spacing. The assessment of composite behaviour within these built-up sections encompasses an investigation into the enhancement of their buckling capacity and the alteration of their corresponding buckling modes. The simplicity of the proposed method expedites comprehensive parametric studies of cold-formed built-up sections, thereby facilitating the exploration of optimal fastener placement and the selection of section geometry.*

1 INTRODUCTION

Over the past few decades, the construction industry has witnessed a significant shift towards the exploration of innovative competitive solutions for midrise construction. Notably, there has been a growing emphasis on leveraging cold-formed steel (CFS) for both the structural framework and the building envelope. This transformative approach to CFS construction methods is reshaping the landscape of low- to mid-rise building projects, offering notable enhancements in quality, construction speed, and environmental sustainability.

The rising demand for CFS sections with greater load-bearing capacities has given rise to a novel application of cold-formed steel. This involves the assembly of multiple individual sections (see Figure 1 (a)) to create composite "built-up" cross-sections (as depicted in Figure 1(b)). These individual profiles are securely interconnected using screws or similar fasteners strategically placed along the member. This innovative approach to forming versatile built-up sections is rapidly broadening the range of applications and fostering creativity in configuring members with enhanced stiffness and strength.

The structural integrity and strength of a built-up CFS member can be accurately assessed only if we have a comprehensive understanding of its behaviour, particularly with regard to buckling. Consequently, there is a pressing need for an efficient analytical tool capable of precisely accounting for the influence of discrete fasteners. In the past decade, extensive research efforts have been dedicated to gaining a deeper insight into built-up sections,

encompassing numerical investigations and experimental studies. This review will provide a succinct overview of these research endeavours, with a specific focus on numerical advancements in the field.

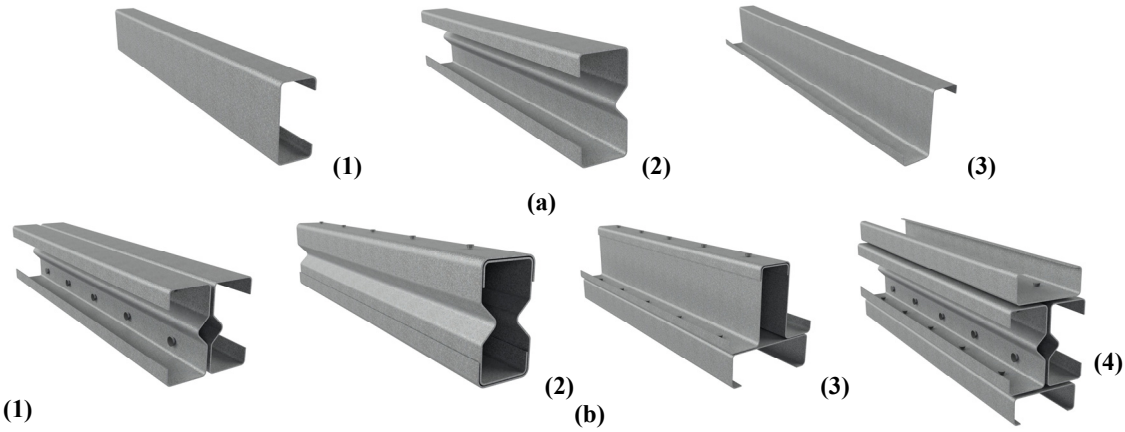

Figure 1. (a) Typical single cold-formed steel sections (b) examples of built-up sections

The most widely employed numerical methods for the buckling analysis of Cold-Formed Steel (CFS) members are the Finite Element (FE) and Finite Strip (FS) methods. These techniques are instrumental in simulating and predicting the structural behaviour of CFS members under various loading conditions, providing valuable insights into their stability and performance. The FSM has found widespread use in the elastic buckling analysis of CFS members due to its numerical efficiency. However, its application is often constrained to simple geometries and uncomplicated end boundary conditions. Recognising these limitations has motivated the development of variants or enrichments of FSM (e.g., [1-3]). Efforts have been made to broaden the applicability of conventional FSM to built-up sections. One approach involves incorporating nodal multi-point constraints that connect desired degrees of freedom (DOFs) from adjacent plate components continuously along the length of the member [4]. Another technique models fasteners as continuous longitudinal solid stiffeners [5]. Despite these attempts, such assumptions may not accurately represent the actual effects of discrete fasteners and might fall short of capturing the level of composite action precisely. These challenges have spurred ongoing research to refine and extend the FSM, ensuring its effectiveness in analysing more complex geometries and boundary conditions encountered in practical structural configurations. Abbasi et al. [6-8] used the compound Finite strip Method (CSM) to model the discrete fasteners as beam elements in the context of the Semi-analytical finite strip method (S-a FSM).

The work of Khezri et al. [2, 9] introduced a novel variation of the Finite Strip Method (FSM) by integrating the one-dimensional formulation of the Generalised RKPM [10, 11] as the approximation tool in the longitudinal direction. This innovative approach demonstrated success in the analysis of bending behaviour for thin plates. Subsequently, the RKP-FSM method was further extended for the analysis of thick plates and laminated composite plates [12, 13]. The generalised reproducing kernel particle method (RKPM) has been applied to various studies, including the transient advection-diffusion-reaction (ADR) equation, a mathematical model that describes transport processes in porous or nonporous materials with time-dependent nonlinear coefficients, intricate geometries, and general initial value and/or boundary conditions [14]. Additionally, the meshless generalised RKPM was utilised in another study focused on the time-dependent advection-diffusion-reaction equation. This equation is relevant to various physical problems involving heat transfer and mass/chemical transport [15].

In this study, the Reproducing Kernel Particle Finite Strip Method (RKP-FSM) is utilised for the buckling analysis of built-up Cold-Formed Steel (CFS) members. The discrete fasteners are represented using constraint equations, where the degrees of freedom of connected nodes are constrained to be identical through equations. The study introduces a straightforward yet accurate framework for analysing built-up sections with diverse cross-sectional compositions and fastener configurations. Section 2 briefly reviews the RKP-FSM, while Section 3 extends the method for the analysis of folded plates. In Section 4, the application of the method is explained for the buckling analysis of built-up sections. Numerical examples in Section 5 demonstrate the accuracy and versatility of the method for the elastic buckling analysis of various built-up CFS sections. Finally, Section 6 provides a summary of the study's outcomes and concludes the paper.

2 GENERALISED REPRODUCING KERNAL PARTICLE FINITE STRIP METHOD (RKP-FSM)

Various adaptations of the Finite Strip Method (FSM) have emerged since its introduction. They all share a common characteristic, which involves creating an estimate for the field variables by combining distinct approximations for longitudinal and transverse components [16]. As a result, a generic function $u(x, y)$ within a domain $\Omega\in\mathbb{R}^2$, with a boundary $\partial\Omega\in\mathbb{R}^2$, can be represented as:

$$u_a(x,y) = F^R(x)G^R(y), \tag{1}$$

where $u_a(x,y)$, in the context of the RKP-FSM, is the constructed approximation obtained by multiplying the approximated longitudinal function via the generalised RKPM, i.e. $F^R(x)$, by the transverse approximation generated using the polynomials functions, i.e. $G^R(y)$. The applied methods and the approximation schemes in each direction are explained briefly in the following subsections.

2.1 Generalised RKPM approximation in the longitudinal direction

In the generalised RKPM, a given function f(x) in a one-dimensional domain ℓ, can be expressed in terms of the functions and its derivatives by the reproducing formula as

$$f^R(x) = \sum_{\eta=0}^{k} \int_{\ell} C^{[\eta]}(x; x-\xi) \frac{1}{a(\xi)} \varphi\left(\frac{|x-\xi|}{a(\xi)}\right) f_{,\eta}(\xi)\,\mathrm{d}\ell, \tag{2}$$

where $f^R(x)$ is the reproduced function, φ is the kernel function, | . | is the absolute value for the distance between x and ξ, and k is the highest order of the considered derivative which is incorporated in the reproduction formula. In equation (2), a is the dilation parameter, and $f_{,k}(\xi)$ is defined as

$$f_{,0}(\xi) = f(\xi), \quad f_{,\eta}(\xi) = \frac{\mathrm{d}^\eta f(\xi)}{\mathrm{d}\xi^\eta}; \quad \forall\eta, \quad \eta = 1,2,\cdots,k. \tag{3}$$

are correction functions that are derived by differentiating the reference correction function $C(x;x\text{-}\xi)$. The reference correction function can be stated as a linear combination of polynomial basis functions given as

$$C(x; x-\xi) = \sum_{i=0}^{m} b_i(x)(x-\xi)^i. \tag{4}$$

In the equation (4), m is the maximum order of the polynomial function which can be reproduced exactly, and $b_i(x)$ is a set of unknown coefficients which can be determined using the completeness condition. Setting

$$\mathbf{p}(x-\xi)=\begin{bmatrix}1 & (x-\xi) & (x-\xi)^2 & \cdots & (x-\xi)^i & \cdots & (x-\xi)^m\end{bmatrix}^{\mathrm{T}}, \tag{5}$$

and

$$\mathbf{b}(x)=\begin{bmatrix}b_0(x) & b_1(x) & b_2(x) & \cdots & b_i(x) & \cdots & b_m(x)\end{bmatrix}^{\mathrm{T}}, \tag{6}$$

results in the reference correction function being restated using matrix notation as

$$C(x;x-\xi)=\mathbf{p}^{\mathrm{T}}(x-\xi)\mathbf{b}(x). \tag{7}$$

The coefficients vector $\mathbf{b}(x)$ should be determined such that the reproduction formula in equation (2) exactly reproduces the polynomials with the required order m. Accordingly, by imposing the completeness condition, these coefficients can be calculated by

$$\mathbf{b}(x)=\mathbf{M}^{-1}(x)\mathbf{H}(0), \tag{8}$$

in which $\mathbf{M}(x)$ is the moment matrix. The required steps for the derivation of the moment matrix are illustrated later in this section.

It is evident that equation (2) is a continuous reproducing kernel approximation, and the considered domain must be discretised using a set of particles to find an approximate solution. By applying trapezoidal rule, the equation becomes

$$f^R(x)=\sum_{I=1}^{NP}\sum_{\eta=0}^{k}C^{[\eta]}(x;x-\xi_I)\varphi\left(\frac{|x-\xi_I|}{a_I}\right)f_{,\eta}(\xi)_{|\xi=\xi_I}\,\Delta x_I, \tag{9}$$

where NP is the number of particles, and Δx_I is the length associated with particle I. Utilising the discretisation scheme, the moment matrix arrays can be determined using the relation

$$\forall 1\le i,j\le m+1:\quad M_{j,i}(x)=\sum_{\eta=0}^{k}S_{j-1,\eta}S_{i-1,\eta}\frac{(i-1)!(j-1)!}{(i-1-\eta)!(j-1-\eta)!}m_{i+j-2\eta-2} \tag{10}$$

where $S_{\alpha,\beta}$ is an index and is set to be

$$S_{\alpha,\beta}=\begin{cases}1 & \beta\le\alpha\\ 0 & \beta>\alpha\end{cases} \tag{11}$$

and

$$\forall\theta\in Z\qquad m_\theta(x)=\begin{cases}\displaystyle\sum_{I=1}^{NP}(x-x_I)^\theta\phi\left(\frac{x-x_I}{a_I}\right)\Delta x_I & \theta\ge 0\\ 1 & \theta<0\end{cases}. \tag{12}$$

In equation (12), ϕ is the kernel function, also known as the window function. Different window function choices are available for adoption as the kernel of the method. Some of these functions have been examined and studied by [17]. In this study, the following window function by setting $l = 9$ has been used [18]:

$$\phi(x)=\begin{cases}\dfrac{(2l+1)!}{2^{2l+1}l!^2}\left(1-x^2\right)^l & |x|\le 1\\ 0 & |x|>1\end{cases}. \tag{13}$$

Since all the required functions in equation (9) can be evaluated numerically using relations (4)-(12), the relations (9) can be restated as

$$f^R(x)=\sum_{\eta=0}^{k}\sum_{I=1}^{NP}\psi_I^{[\eta]}(x)f_{,\eta}^I, \tag{14}$$

where

$$\psi_I^{[\eta]}(x)=C^{[\eta]}(x;x-x_I)\phi\left(\frac{x-x_I}{a_I}\right)\Delta x_I, \tag{15}$$

and $\psi_I^{[\eta]}(x)$ are the particle I's associated shape functions. The number of shape functions at each node is dependent on the order of the derivative considered in the reproducing formula. The shape functions obtained will be employed in the longitudinal direction to approximate the field variables considered. In the present study, only the first derivative of the function will be incorporated in the approximation function. Accordingly, by setting k = 1, two sets of functions will be constructed. Schematic views of these functions in an arbitrary domain with uniform discretisation scheme using 11 particles are presented in Figure 2.

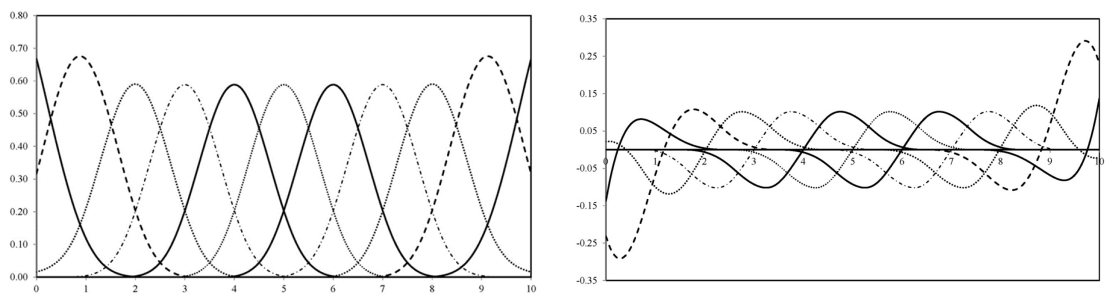

(a) (b)

Figure 2. Generalised RKPM shape function associated with the (a) function $\psi_I^{[0]}(x)$, and (b) first derivative of the function $\psi_I^{[1]}(x)$

2.2 Cubic polynomial interpolation in the transverse direction

As in the conventional SFSM, a cubic polynomial interpolation will be adopted in the transverse direction for the displacements normal to the plane of the strip. These shape functions are [19]:

$$\begin{cases}N_1=1-3\bar{y}^2+2\bar{y}^3\\ N_2=y\left(1-2\bar{y}+\bar{y}^2\right)\\ N_3=\left(3\bar{y}^2-2\bar{y}^3\right)\\ N_4=y\left(\bar{y}^2-\bar{y}\right),\end{cases};\bar{y}=\frac{y}{b} \tag{16}$$

in which b is the width of the strip. Of course, the shape functions presented are for lower order (LO2) and higher order strips such as (HO2) and (HO3), or strips with augmentation of bubble functions could be constructed by replacing and adding proper shape functions [20]. For the in-plane displacements, linear interpolations are utilised in the transverse direction, viz.

$$\begin{cases} N_5 = 1 - \bar{y} \\ N_6 = \bar{y}. \end{cases} \tag{17}$$

3 BUCKLING ANALYSIS OF THIN-WALLED MEMBERS

In the reproducing kernel particle finite strip method (RKP-FSM) a thin-walled member, such as the lipped channel shown in Figure 3(a), is discretised into longitudinal strips. In Figure 3(b)-(c), a single strip discretisation, strip dimensions, and applied edge tractions are highlighted. In the longitudinal direction, each nodal line is further subdivided into $m+1$ particles. Each section knot has eight degrees of freedom corresponding to the two out-of-plane deformations and their derivatives w, $w_{,x}$, θ_x and $\theta_{x,x}$, two in-plane deformations and their derivatives u, $u_{,x}$, v, $v_{,x}$. It is noteworthy that in the proposed RKP-FSM, because a meshfree method's shape functions are adopted, the placement of the particles can be non-uniform and in any desired manner. This feature of the method allows for more flexibility in the mesh generation process and also for possible local refinements of the utilised meshes.

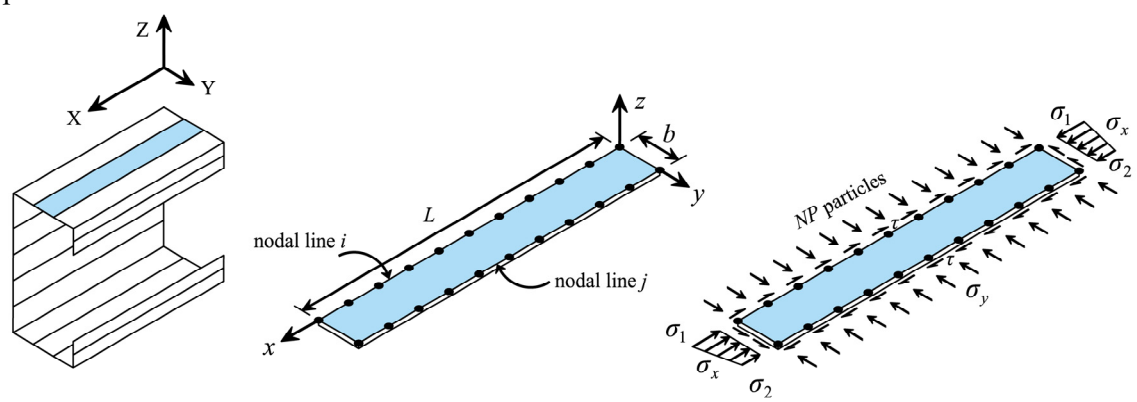

(a) (b) (c)

Figure 3. (a) Finite strip discretization, (b) a basic RKPFSM's strip (c) state of stress in a strip

3.1 Buckling displacement functions

The in-plane buckling displacements u and v of an RKP strip can be expressed in terms of transverse polynomials, and longitudinal generalised RKPM shape functions as

$$\begin{Bmatrix} u \\ v \end{Bmatrix} = \begin{bmatrix} N_5 & & N_6 & \\ & N_5 & & N_6 \end{bmatrix} \begin{bmatrix} \boldsymbol{\psi}^{[0]} & \boldsymbol{\psi}^{[1]} & & & & & & \\ & & \boldsymbol{\psi}^{[0]} & \boldsymbol{\psi}^{[1]} & & & & \\ & & & & \boldsymbol{\psi}^{[0]} & \boldsymbol{\psi}^{[1]} & & \\ & & & & & & \boldsymbol{\psi}^{[0]} & \boldsymbol{\psi}^{[1]} \end{bmatrix} \begin{Bmatrix} \mathbf{u}^i \\ \mathbf{u}^i_{,x} \\ \mathbf{v}^i \\ \mathbf{v}^i_{,x} \\ \mathbf{u}^j \\ \mathbf{u}^j_{,x} \\ \mathbf{v}^j \\ \mathbf{v}^j_{,x} \end{Bmatrix} = \mathbf{N}_M \boldsymbol{\psi}_M \mathbf{d}_M, \tag{18}$$

where

$$\boldsymbol{\psi}^{[0]} = \begin{bmatrix} \psi_1^{[0]} & \psi_2^{[0]} & \cdots & \psi_{m+1}^{[0]} \end{bmatrix}, \quad \boldsymbol{\psi}^{[1]} = \begin{bmatrix} \psi_1^{[1]} & \psi_2^{[1]} & \cdots & \psi_{m+1}^{[1]} \end{bmatrix}, \tag{19}$$

are the row vectors of the first and second type shape functions of the generalized RKPM, which are obtained via equation (15). The membrane nodal value vector, denoted as $\mathbf{d}_M$, is composed

of the nodal displacement coefficient vectors, which include $\mathbf{u}^i$, $\mathbf{u}^i_{,x}$, $\mathbf{u}^j$, $\mathbf{u}^j_{,x}$, $\mathbf{v}^i$, $\mathbf{v}^i_{,x}$, $\mathbf{v}^j$, and $\mathbf{v}^j_{,x}$, each of them containing m+1 terms. Here, the superscripts i and j indicate the respective nodal lines on which these nodal values are defined. Similarly, the flexural displacement function w for buckling displacements normal to the plane of the RKP strip is expressed as follows:

$$w = \begin{bmatrix} N_1 & N_2 & N_3 & N_4 \end{bmatrix} \begin{bmatrix} \boldsymbol{\psi}^{[0]} & \boldsymbol{\psi}^{[1]} & & & & & & \\ & & \boldsymbol{\psi}^{[0]} & \boldsymbol{\psi}^{[1]} & & & & \\ & & & & \boldsymbol{\psi}^{[0]} & \boldsymbol{\psi}^{[1]} & & \\ & & & & & & \boldsymbol{\psi}^{[0]} & \boldsymbol{\psi}^{[1]} \end{bmatrix} \begin{Bmatrix} \mathbf{w}^i \\ \mathbf{w}^i_{,x} \\ \boldsymbol{\theta}^i_x \\ \boldsymbol{\theta}^i_{x,x} \\ \mathbf{w}^j \\ \mathbf{w}^j_{,x} \\ \boldsymbol{\theta}^j_x \\ \boldsymbol{\theta}^j_{x,x} \end{Bmatrix} = \mathbf{N}_F \boldsymbol{\psi}_F \mathbf{d}_F . \tag{20}$$

The flexural nodal value vector, denoted as $\mathbf{d}_F$, is composed of the nodal displacement coefficient vectors, including $\mathbf{w}^i$, $\mathbf{w}^i_{,x}$, $\mathbf{w}^j$, $\mathbf{w}^j_{,x}$, $\boldsymbol{\theta}^i_x$, $\boldsymbol{\theta}^i_{x,x}$, $\boldsymbol{\theta}^j_x$, and $\boldsymbol{\theta}^j_{x,x}$, with each vector containing m+1 terms. In equations (18) and (20), the subscripts M and F are used to represent membrane and flexural displacements, respectively.

3.2 Membrane stiffness and stability matrices

The flat strip is assumed to maintain its flat shape under the applied stresses, until it reaches the point of buckling. The strain energy associated with the membrane deformation of this strip is expressed as follows:

$$U_M = \frac{1}{2}\int_L\int_b \boldsymbol{\sigma}_M^T \boldsymbol{\varepsilon}_M t \,\mathrm{d}x\mathrm{d}y = \frac{1}{2}\mathbf{d}_M^{\mathrm{T}} \left(\int_L\int_b \mathbf{B}_M^T \mathbf{D}_M \mathbf{B}_M t \,\mathrm{d}x\mathrm{d}y \right) \mathbf{d}_M = \frac{1}{2}\mathbf{d}_M^{\mathrm{T}} \mathbf{K}_M \mathbf{d}_M , \tag{21}$$

in which $\mathbf{K}_M$ is the membrane stiffness matrix, $\mathbf{d}_M$ is the vector of membrane DOFs and

$$\boldsymbol{\sigma}_M = \begin{bmatrix} \sigma_x & \sigma_y & \sigma_{xy} \end{bmatrix}^{\mathrm{T}}, \quad \boldsymbol{\varepsilon}_M = \begin{bmatrix} \partial u/\partial x & \partial v/\partial y & \partial u/\partial y + \partial v/\partial x \end{bmatrix}^{\mathrm{T}} . \tag{22}$$

$\mathbf{D}_M$ is the membrane property matrix, and the membrane strain matrix $\mathbf{B}_M$ can be obtained by differentiating the displacement function in equation (18).

The reduction in potential energy of the membrane forces during buckling, assuming that the destabilising effect of stresses σ_y and τ is negligible, can be calculated using the following expression:

$$V_M = \frac{1}{2}\int_L\int_b \sigma_x \left[\left(\partial u/\partial x \right)^2 + \left(\partial v/\partial y \right)^2 \right] t \,\mathrm{d}y\mathrm{d}x = \frac{1}{2}\mathbf{d}_M^{\mathrm{T}} \mathbf{G}_M \mathbf{d}_M , \tag{23}$$

where $\mathbf{G}_M$ is the membrane stability matrix.

3.3 Flexural stiffness and stability matrices

The flexural strain energy of a plate strip under the state of stress resulting from the buckling-caused deformations can be stated as

$$U_F = \frac{1}{2}\int_L\int_b \boldsymbol{\sigma}_F^T \boldsymbol{\varepsilon}_F \,\mathrm{d}x\mathrm{d}y = \frac{1}{2}\mathbf{d}_F^T \left(\int_L\int_b \mathbf{B}_F^T \mathbf{D}_F \mathbf{B}_F \,\mathrm{d}x\mathrm{d}y \right) \mathbf{d}_F = \frac{1}{2}\mathbf{d}_F^T \mathbf{K}_F \mathbf{d}_F , \tag{24}$$

in which $\mathbf{K}_F$ is the flexural stiffness matrix, $\mathbf{d}_F$ is the vector of flexural degrees of freedom and

$$\boldsymbol{\sigma}_F = \begin{bmatrix} \mathbf{M}_x & \mathbf{M}_y & \mathbf{M}_{xy} \end{bmatrix}^{\mathrm{T}}, \quad \boldsymbol{\varepsilon}_M = \begin{bmatrix} \frac{-\partial^2 w}{\partial x^2} & \frac{-\partial^2 w}{\partial y^2} & \frac{2\partial^2 w}{\partial x \partial y} \end{bmatrix}^{\mathrm{T}}. \tag{25}$$

$\mathbf{D}_F$ is the flexural property matrix. The decrease in the potential energy of the in-plane stresses caused by the flexural buckling deformation will be taken as

$$V_F = \frac{1}{2}\int_L\int_b \left[\sigma_x \left(\frac{\partial w}{\partial x}\right)^2 + \sigma_y \left(\frac{\partial w}{\partial y}\right)^2 + 2\tau \left(\frac{\partial w}{\partial x}\right)\left(\frac{\partial w}{\partial y}\right) \right] t \mathrm{d}y \mathrm{d}x = \frac{1}{2}\mathbf{d}_F^{\mathrm{T}} \mathbf{G}_F \mathbf{d}_F, \tag{26}$$

in which $\mathbf{G}_F$ is the flexural stability matrix.

3.4 Global stiffness and stability matrices and assembly

To form the global elastic (**K**) and geometric stiffness (**G**) matrices each individual strip must be transformed from local to global coordinates and then assembled. The deformation in the local axes system $\boldsymbol{\delta}$ are related to those in the global axes $\boldsymbol{\Delta}$ by

$$\boldsymbol{\delta} = \mathbf{R}\boldsymbol{\Delta} \tag{27}$$

where

$$\delta = \begin{bmatrix} \mathbf{u}^i & \mathbf{u}^i_{,x} & \mathbf{v}^i & \mathbf{v}^i_{,x} & \mathbf{w}^i & \mathbf{w}^i_{,x} & \boldsymbol{\theta}^i_x & \boldsymbol{\theta}^i_{x,x} & \mathbf{u}^j & \mathbf{u}^j_{,x} & \mathbf{v}^j & \mathbf{v}^j_{,x} & \mathbf{w}^j & \mathbf{w}^j_{,x} & \boldsymbol{\theta}^j_x & \boldsymbol{\theta}^j_{x,x} \end{bmatrix}^{\mathrm{T}} \tag{28}$$

$$\Delta = \begin{bmatrix} \mathbf{U}^i & \mathbf{U}^i_{,X} & \mathbf{V}^i & \mathbf{V}^i_{,X} & \mathbf{W}^i & \mathbf{W}^i_{,X} & \boldsymbol{\Theta}^i_x & \boldsymbol{\Theta}^i_{x,x} & \mathbf{U}^j & \mathbf{U}^j_{,x} & \mathbf{V}^j & \mathbf{V}^j_{,x} & \mathbf{W}^j & \mathbf{W}^j_{,x} & \boldsymbol{\Theta}^j_x & \boldsymbol{\Theta}^j_{x,x} \end{bmatrix}^{\mathrm{T}} \tag{29}$$

and,

$$\mathbf{R} = \begin{bmatrix} \mathbf{r} & \\ & \mathbf{r} \end{bmatrix}, \quad \text{in which } \mathbf{r} = \begin{bmatrix} \mathbf{I} & & & \\ & \mathbf{I}\cos\alpha & \mathbf{I}\sin\alpha & \\ & -\mathbf{I}\sin\alpha & \mathbf{I}\cos\alpha & \\ & & & \mathbf{I} \end{bmatrix}. \tag{30}$$

I is an idendity matrix of size $(2\times(m+1)) \times (2\times(m+1))$. By assembling the transformed stiffness and stability matrices of the strips and obtaining the global stiffness **K** and stability **G** matrices, utilising the principle of stationary total potential, the buckling equation takes the familiar form

$$(\mathbf{K} - \lambda\mathbf{G})\Delta = \mathbf{0}. \tag{31}$$

For buckling, the determinant **K**-λ**G** must be vanished, which can be solved for the buckling load factor using standard eigenvalue solvers.

4 BUCKLING ANALYSIS OF BUILT-UP MEMBERS

The approach employed for analysing the buckling behaviour of built-up members involves a detailed discretisation process. Each constituent section, denoted as *A* and *B* (see Figure 4(a)), undergoes independent section discretization to capture its unique structural characteristics. A critical aspect of this process is the introduction of nodal lines within each section, precisely aligned with the locations of fasteners (Figure 4(b). These nodal lines, one for each section, serve as basis for the introduction of connection points (two ends of fasteners). Additionally, for longitudinal discretisation, particles (nodes) are placed along these nodal lines. As shown in Figure 4(c), longitudinal discretisation entails the placement of regular nodes at equal intervals, with additional particles added at the exact locations of the fasteners. Although resulting in an irregular distribution of nodes, the utilisation of a mesh-free method in the longitudinal direction empowers the approach to effectively handle such irregularities.

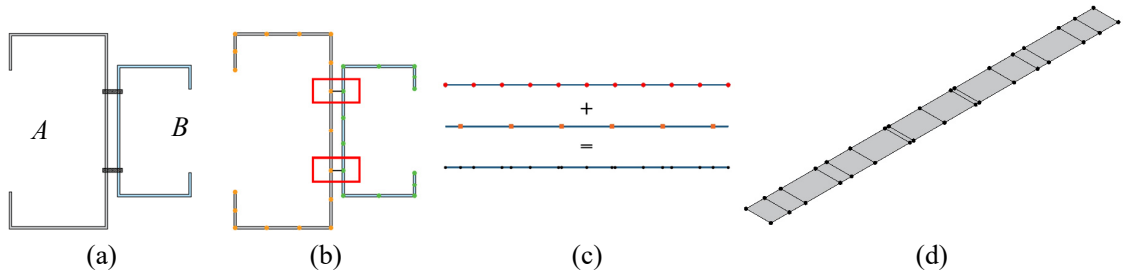

Figure 4. (a) Built-up members (b) FS discretisation and connected nodal lines (c) longitudinal discretisation of the connected nodal lines consisting of regular and connection particles (d) single strip discretisation

Thus, utilising the aforementioned discretisation scheme, the buckling equation (31) for these sections can be stated separately as

$$\left(\mathbf{K}^A - \lambda \mathbf{G}^A\right)\Delta^A = \mathbf{0} \quad \text{and} \quad \left(\mathbf{K}^B - \lambda \mathbf{G}^B\right)\Delta^B = \mathbf{0}, \tag{32}$$

or using matrix notation as:

$$\left(\begin{bmatrix} \mathbf{K}^A & \mathbf{0} \\ \mathbf{0} & \mathbf{K}^B \end{bmatrix} - \lambda \begin{bmatrix} \mathbf{G}^A & \mathbf{0} \\ \mathbf{0} & \mathbf{G}^B \end{bmatrix}\right)\begin{bmatrix} \Delta^A \\ \Delta^B \end{bmatrix} = \mathbf{0}. \tag{33}$$

The degrees of freedom (DOFs) in each section are systematically numbered according to the following protocol:

(1) The first category encompasses the DOFs where essential boundary conditions are specified. These degrees of freedom, along with their corresponding components, are denoted by a subscript '*e*'.
(2) The second group comprises the DOFs situated at the connection nodes. Notably, since an identical number of connection nodes is employed in both sections, the count of connection DOFs remains consistent for both sections. Variables associated with these DOFs are designated with a subscript '*c*'.
(3) Lastly, the remaining DOFs are represented with the subscript '*r*'.

Employing this designated numbering scheme, the matrices in equation (33) undergo a partitioning process, resulting in a structured equation form as follows:

$$\left(\begin{bmatrix} \mathbf{K}^A_{ee} & \mathbf{K}^A_{ec} & \mathbf{K}^A_{er} & \mathbf{0} & \mathbf{0} & \mathbf{0} \\ \mathbf{K}^A_{ce} & \mathbf{K}^A_{cc} & \mathbf{K}^A_{cr} & \mathbf{0} & \mathbf{0} & \mathbf{0} \\ \mathbf{K}^A_{re} & \mathbf{K}^A_{rc} & \mathbf{K}^A_{rr} & \mathbf{0} & \mathbf{0} & \mathbf{0} \\ \mathbf{0} & \mathbf{0} & \mathbf{0} & \mathbf{K}^B_{ee} & \mathbf{K}^B_{ec} & \mathbf{K}^B_{er} \\ \mathbf{0} & \mathbf{0} & \mathbf{0} & \mathbf{K}^B_{ce} & \mathbf{K}^B_{cc} & \mathbf{K}^B_{cr} \\ \mathbf{0} & \mathbf{0} & \mathbf{0} & \mathbf{K}^B_{re} & \mathbf{K}^B_{rc} & \mathbf{K}^B_{rr} \end{bmatrix} - \lambda \begin{bmatrix} \mathbf{G}^A_{ee} & \mathbf{G}^A_{ec} & \mathbf{G}^A_{er} & \mathbf{0} & \mathbf{0} & \mathbf{0} \\ \mathbf{G}^A_{ce} & \mathbf{G}^A_{cc} & \mathbf{G}^A_{cr} & \mathbf{0} & \mathbf{0} & \mathbf{0} \\ \mathbf{G}^A_{re} & \mathbf{G}^A_{rc} & \mathbf{G}^A_{rr} & \mathbf{0} & \mathbf{0} & \mathbf{0} \\ \mathbf{0} & \mathbf{0} & \mathbf{0} & \mathbf{G}^B_{ee} & \mathbf{G}^B_{ec} & \mathbf{G}^B_{er} \\ \mathbf{0} & \mathbf{0} & \mathbf{0} & \mathbf{G}^B_{ce} & \mathbf{G}^B_{cc} & \mathbf{G}^B_{cr} \\ \mathbf{0} & \mathbf{0} & \mathbf{0} & \mathbf{G}^B_{re} & \mathbf{G}^B_{rc} & \mathbf{G}^B_{rr} \end{bmatrix}\right)\begin{bmatrix} \Delta^A_e \\ \Delta^A_c \\ \Delta^A_r \\ \Delta^B_e \\ \Delta^B_c \\ \Delta^B_r \end{bmatrix} = \mathbf{0}. \tag{34}$$

In the next step, all of the DOFs in both sections are numbered again using the same numbering pattern which was used for numbering each section. The numbering is performed such that those DOFs which are located on the connection points, corresponding to the same component of the displacement, (one in section *A* and the other in section *B*) are placed in sequential order. Utilising the global partitioning order, equation (34) takes the form

$$\left(\begin{bmatrix} \mathbf{K}_{ee}^{A} & \mathbf{0} & \mathbf{K}_{ec}^{A} & \mathbf{0} & \mathbf{K}_{er}^{A} & \mathbf{0} \\ \mathbf{0} & \mathbf{K}_{ee}^{B} & \mathbf{0} & \mathbf{K}_{ec}^{B} & \mathbf{0} & \mathbf{K}_{er}^{B} \\ \mathbf{K}_{ce}^{A} & \mathbf{0} & \mathbf{K}_{cc}^{A} & \mathbf{0} & \mathbf{K}_{cr}^{A} & \mathbf{0} \\ \mathbf{0} & \mathbf{K}_{ce}^{B} & \mathbf{0} & \mathbf{K}_{cc}^{B} & \mathbf{0} & \mathbf{K}_{cr}^{B} \\ \mathbf{K}_{re}^{A} & \mathbf{0} & \mathbf{K}_{rc}^{A} & \mathbf{0} & \mathbf{K}_{rr}^{A} & \mathbf{0} \\ \mathbf{0} & \mathbf{K}_{re}^{B} & \mathbf{0} & \mathbf{K}_{rc}^{B} & \mathbf{0} & \mathbf{K}_{rr}^{B} \end{bmatrix} - \lambda \begin{bmatrix} \mathbf{G}_{ee}^{A} & \mathbf{0} & \mathbf{G}_{ec}^{A} & \mathbf{0} & \mathbf{G}_{er}^{A} & \mathbf{0} \\ \mathbf{0} & \mathbf{G}_{ee}^{B} & \mathbf{0} & \mathbf{G}_{ec}^{B} & \mathbf{0} & \mathbf{G}_{er}^{B} \\ \mathbf{G}_{ce}^{A} & \mathbf{0} & \mathbf{G}_{cc}^{A} & \mathbf{0} & \mathbf{G}_{cr}^{A} & \mathbf{0} \\ \mathbf{0} & \mathbf{G}_{ce}^{B} & \mathbf{0} & \mathbf{G}_{cc}^{B} & \mathbf{0} & \mathbf{G}_{cr}^{B} \\ \mathbf{G}_{re}^{A} & \mathbf{0} & \mathbf{G}_{rc}^{A} & \mathbf{0} & \mathbf{G}_{rr}^{A} & \mathbf{0} \\ \mathbf{0} & \mathbf{G}_{re}^{B} & \mathbf{0} & \mathbf{G}_{rc}^{B} & \mathbf{0} & \mathbf{G}_{rr}^{B} \end{bmatrix}\right) \begin{bmatrix} \Delta_{e}^{A} \\ \Delta_{e}^{B} \\ \Delta_{c}^{A} \\ \Delta_{c}^{B} \\ \Delta_{r}^{A} \\ \Delta_{r}^{B} \end{bmatrix} = \mathbf{0}. \tag{35}$$

Because the nodal displacements $\Delta^{A}{}_{e}$ and $\Delta^{B}{}_{e}$ are associated with essential boundary conditions and assuming that the prescribed boundary conditions are equal to zero, then

$$\Delta_{e}^{A} = \Delta_{e}^{B} = \mathbf{0}. \tag{36}$$

Also, because $\Delta^{A}{}_{c}$ and $\Delta^{B}{}_{c}$ are associated with DOFs which are located on connection nodes and are basically the same displacement values, it can be assumed that

$$\Delta_{c}^{A} = \Delta_{c}^{B}. \tag{37}$$

Considering the equations (36) and (37), the buckling equation takes the form

$$\left(\begin{bmatrix} \mathbf{K}_{cc}^{A} + \mathbf{K}_{cc}^{B} & \mathbf{K}_{cr}^{A} & \mathbf{K}_{cr}^{B} \\ \mathbf{K}_{rc}^{A} & \mathbf{K}_{rr}^{A} & \mathbf{0} \\ \mathbf{K}_{rc}^{B} & \mathbf{0} & \mathbf{K}_{rr}^{B} \end{bmatrix} - \lambda \begin{bmatrix} \mathbf{G}_{cc}^{A} + \mathbf{G}_{cc}^{B} & \mathbf{G}_{cr}^{A} & \mathbf{G}_{cr}^{B} \\ \mathbf{G}_{rc}^{A} & \mathbf{G}_{rr}^{A} & \mathbf{0} \\ \mathbf{G}_{rc}^{B} & \mathbf{0} & \mathbf{G}_{rr}^{B} \end{bmatrix}\right) \begin{bmatrix} \Delta_{c}^{A} \\ \Delta_{r}^{A} \\ \Delta_{r}^{B} \end{bmatrix} = \mathbf{0}. \tag{38}$$

By solving equation (38), the buckling load factor λ can be determined.

5 NUMERICAL EXAMPLES

In this section, numerical illustrations are presented to validate the applicability of the proposed numerical techniques for the elastic buckling analysis of built-up sections with discrete fasteners. The RKP-FSM method is employed for modelling the built-up members, while the connections between the constituent sections are enforced using the modified collocation method outlined in section 4.

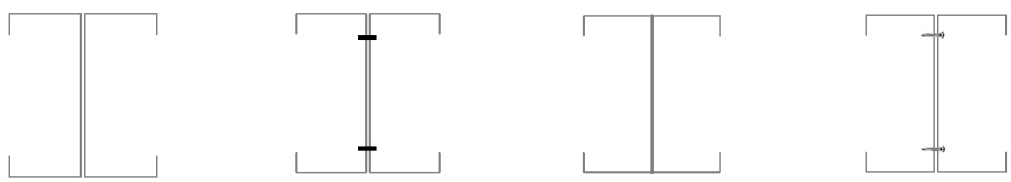

(a) (b) (c) (d)

Figure 5. Different levels of composite actions: (a) non-composite, (b) partially composite with continuous connections, (c) fully-composite, (d) partially composite with discrete connections

The accuracy of the results obtained is verified through comparisons with solutions from Finite Element (FE) and S-a FS (Semi-Analytical Finite Strip) methods. Although the S-a FSM cannot directly model discrete fasteners, it offers lower and upper bounds for the buckling problem of built-up sections. The lower bound is derived when no composite action is assumed between the sections, as depicted in Figure 5(a). This implies that the buckling load for compound sections is twice the critical load determined for a single section. Conversely, an upper bound for the solution is achieved by assuming a continuous connection at the fastener locations along the member length, as shown in Figure 5(b). In an S-a FSM analysis, this condition can be enforced by placing two nodes at the positions of fasteners (one on each section) and constraining their corresponding degrees of freedom to be equal. A fully composite

state is realised when the connected component plates of the sections are fully fused and modelled as a single shared component with a thickness of 2t, as illustrated in Figure 5(c). The partially composite state with discrete fasteners (Figure 5(d)) can be modelled using the proposed RKP-FSM or the finite element analysis.

5.1 Example 1: Buckling analysis of channel sections

In the initial example, the performance of the RKP-FSM is evaluated in the buckling analysis of thin-walled sections. This is notable as it represents the first development of the RKP-FSM for analysing members with folded plate elements. Previous applications of the method have primarily focused on the bending and buckling of plates [2, 9, 21], as well as on the analysis of laminated composites [12, 13], functionally graded materials [22]. For this analysis, a single channel section with the cross-sectional dimensions shown in Figure 6(a) was selected and analysed under uniform compressive loads. The FS discretisation of the cross-section is presented in Figure 6(b). It is assumed that the sections are constructed from cold-formed steel with material properties, specifically Young's modulus (E) of 210 GPa, a yield strength (f_y) of 500 MPa, and a Poisson's ratio (ν) of 0.3.

Figure 6. (a) Geometry of a lipped channel section and (b) utilised FS discretisation

A series of analyses are conducted using RKP-FSM with the number of particles in the longitudinal direction N_P = 20. It is noted that for some of the considered lengths, a lower number of particles also yields accurate results. The buckling load curves obtained for simply-supported and clamped boundary conditions are shown in Figure 7(a) and Figure 7(b), respectively. The S-a FSM implemented in the CUFSM software [23] is utilised to validate the RKP-FSM results. The number of longitudinal trigonometric terms is selected sufficiently large to capture the member correct buckling behaviour.

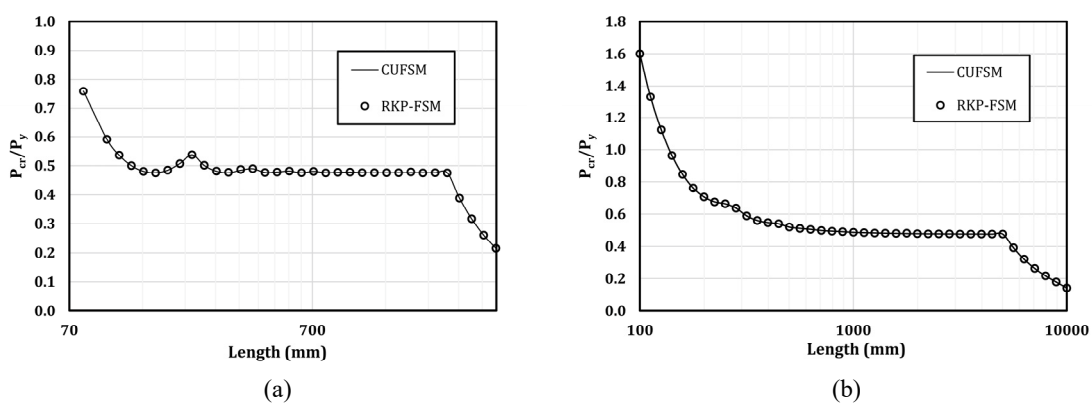

Figure 7. Buckling load curves of the single-channel columns; (a) simply supported, and (b) clamped boundary conditions.

The results, as presented in Figure 7, indicate excellent agreement among the methods, thereby confirming the suitability of the RKP-FSM for the analysis of thin-walled members.

Furthermore, in the analyses conducted using the RKP-FSM for columns under (S-S) boundary conditions, the first mode shapes observed, along with their corresponding buckling load factors for three different lengths, are presented in Figure 8(a). Additionally, the results of finite element (FE) analyses performed using Abaqus [24] are included in Figure 8(b) for verification, and they exhibit similar mode shapes and critical buckling load factors to those obtained using the RKP-FSM.

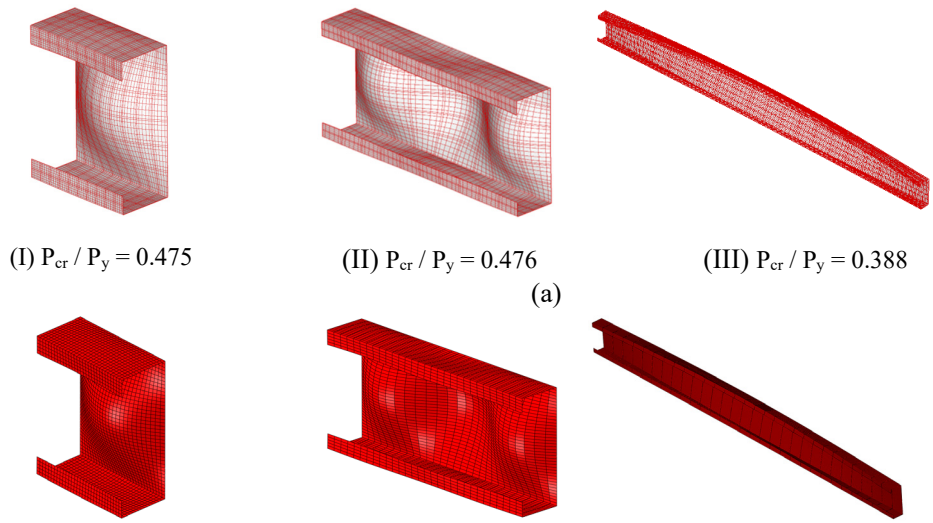

(I) P_{cr} / P_y = 0.475 (II) P_{cr} / P_y = 0.476 (III) P_{cr} / P_y = 0.388

(a)

(I) P_{cr} / P_y = 0.440 (II) P_{cr} / P_y = 0.461 (III) P_{cr} / P_y = 0.390

(b)

Figure 8. Buckling modes shapes and critical buckling loads for members of length: (I) L = 160 mm (II) L = 445 mm (III) L = 2800 mm, (a) RKP-FSM, and (b) FEM results

5.3 Example 2: Buckling analysis back-to-back channels sections

In this example, the analysis focuses on single-span built-up columns comprised of two channels. The investigation considers a built-up I-section with the same geometry and assembly as illustrated in Figure 9. The RKP-FSM is applied with a specified fastener spacing set as $s = (L\text{-}2a)/5$, $a = 30$ mm, and both ends of the column are assumed to be simply supported. The obtained results for simply supported boundary conditions (S-S) are presented in Figure 10. These results are then compared with fully composite (CUFSM-FC) and non-composite (CUFSM-Single) curves, which serve as theoretical upper and lower bounds, respectively, in the same figures. As mentioned earlier, an upper bound for the partially-composite solution (CUFSM-Double) can be established by assuming a continuous connection at the fastener locations along the member length. In the analysis using S-a FSM, this condition is enforced by placing two nodes at the positions of the fasteners (one on each section) and constraining their corresponding degrees of freedom to be equal. For the depicted built section in Figure 9(b), this upper limit can be determined by constraining two pairs of nodes, specifically (7,23) and (10,26). The solutions based on this assumption should align with the analysis results of the built-up section with discrete fasteners when the spacing between the fasteners (s in the longitudinal direction) approaches zero. This upper bound serves as a reference for understanding the influence of discrete fasteners on the structural behaviour of the built-up section. An intermediate composite level, as depicted in Figure 5(d), is considered by modelling discrete connections. This configuration represents a realistic composite state that falls between the fully-composite and non-composite states. The proposed Reproducing Kernel Particle Finite Strip Method (RKP-FSM) is employed to model this partially composite state with discrete connections. This modelling approach (RKP-FSM-Double) allows for a more nuanced and

accurate representation of the structural behaviour, capturing the influence of discrete connections on the overall composite state.

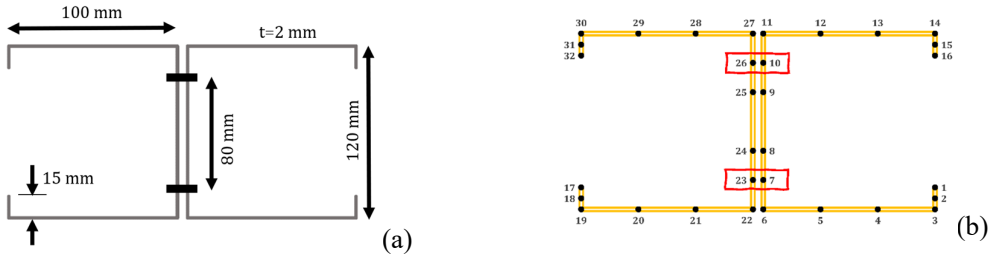

Figure 9. The considered built-up I-section: (a) geometry, (b) finite strip discretisation.

Analysing the buckling load curve (Figure 10) reveals that the considered built-up section is susceptible to both local and distortional buckling. The curve exhibits multiple local and distortional minima, with the distortional minima generally lower than the local minima. This characteristic suggests that the built-up section is prone to different modes of instability, emphasising the importance of considering both local and distortional buckling phenomena in the design and analysis of such structures. Understanding the distribution and magnitudes of these minima is crucial for predicting the behaviour and performance of the built-up section under various loading conditions.

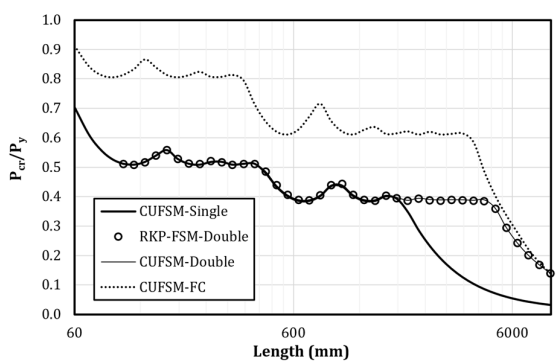

Figure 10. buckling load curves of the built-up I section with S-S end conditions and fastener spacing $s = (L\text{-}2a)/5$

In the RKP-FSM analyses, typical first mode shapes and buckling loads observed for local and global buckling of the considered built-up sections are presented in Figure 11. These results are presented for members with length L = 220 mm, 700 mm, and 2240 mm, and then compared with those obtained using Finite Element (FE) analysis (ABAQUS). The figures include the results of FE analyses for verification, revealing similar mode shapes/load factors with the RKP-FSM. This agreement between RKP-FSM and FE results indicates the effectiveness and reliability of the proposed method in capturing the buckling behaviour of the built-up sections. The inclusion of FE results serves to validate and strengthen the confidence in the accuracy of the RKP-FSM outcomes.

5.3 Example 3: Buckling analysis of built-up members with multiple sections

In this example, a more intricate built-up section is under consideration, as illustrated in Figure 12(a). This composite section is composed of four lipped channels with longitudinal stiffeners (LC-LS) connected by employing a series of discrete web-to-flange and web-to-web fasteners. The finite strip discretisation of the cross-section is presented in Figure 12(b), showcasing the utilised division of the section for analysis.

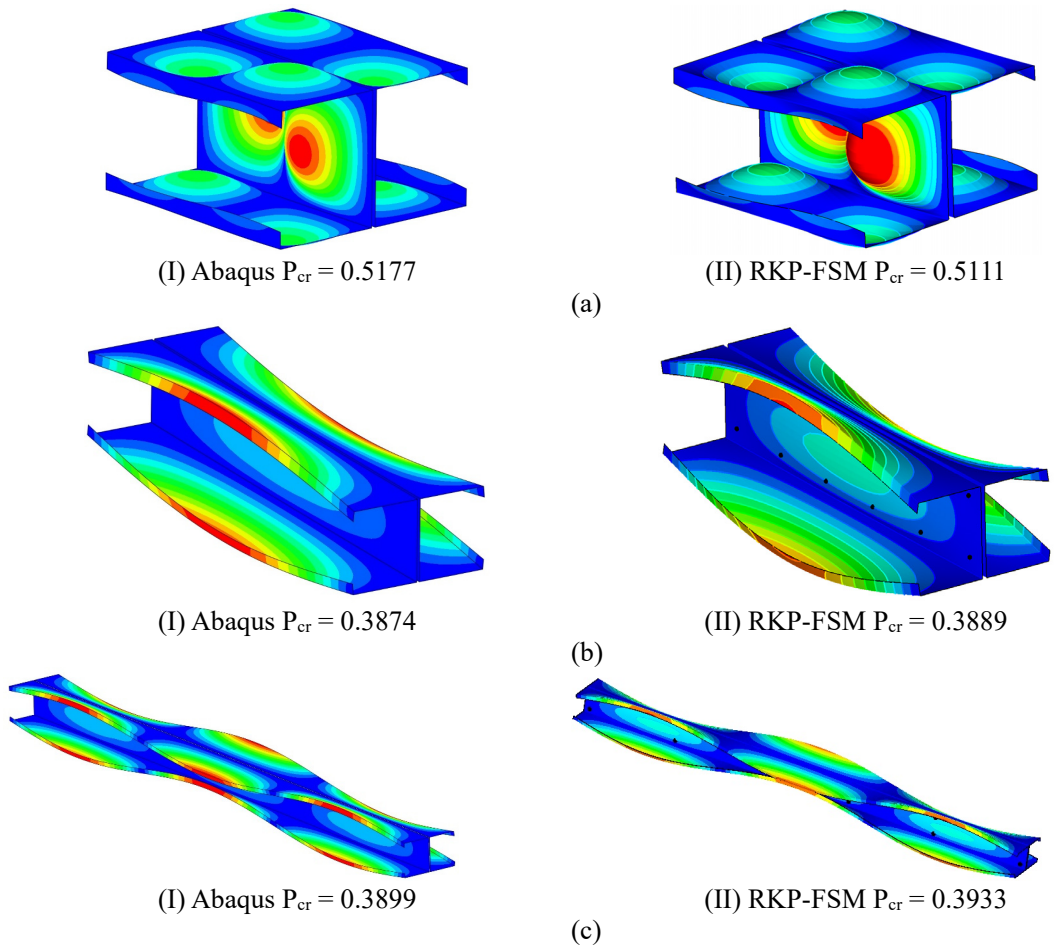

Figure 11. Comparison of buckling loads and mode shapes obtained using Abaqus and RKP-FSM for lengths (a) L = 220 mm, (b) = 700 mm , (c) L = 2240

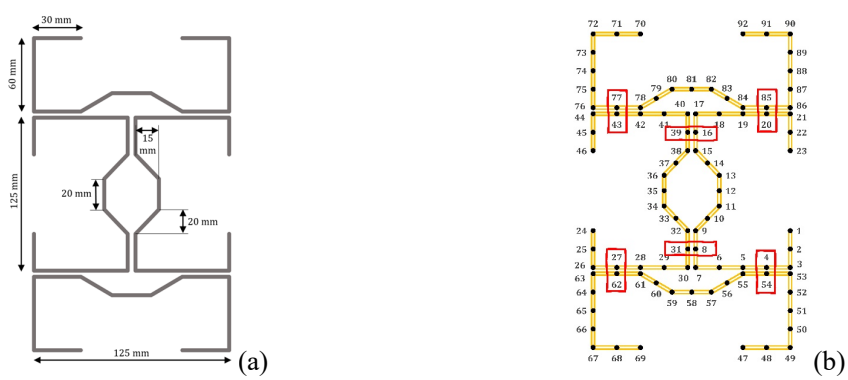

Figure 12. The considered member with multiple sections: (a) geometry, (b) FS discretisation

The built-up column is subjected to uniform compression with simply-supported boundary conditions at both ends (S-S), and the corresponding signature curves are derived. In Figure 13, a comparative analysis is presented between the results obtained from RKP-FSM and CUFSM simulations for varying values of *s,* specifically $s = (L\text{-}2a)$, $s = (L\text{-}2a)/3$, and $s = (L\text{-}2a)/5$. Notably, the partial composite approach embraced by CUFSM yields distinct outcomes compared to the discrete modelling of fasteners using RKP-FSM. As the spacing of fasteners diminishes, the results obtained via RKP-FSM converge towards those acquired through continuous connections. This trend underscores a critical observation: in the realm of global

buckling, the buckling load obtained through the discrete representation of fasteners as individual points diverges from the outcomes obtained via a continuous approach. This reaffirms that even in the global buckling region, the choice of modelling fasteners as discrete points versus a continuous approach can lead to disparate buckling load predictions.

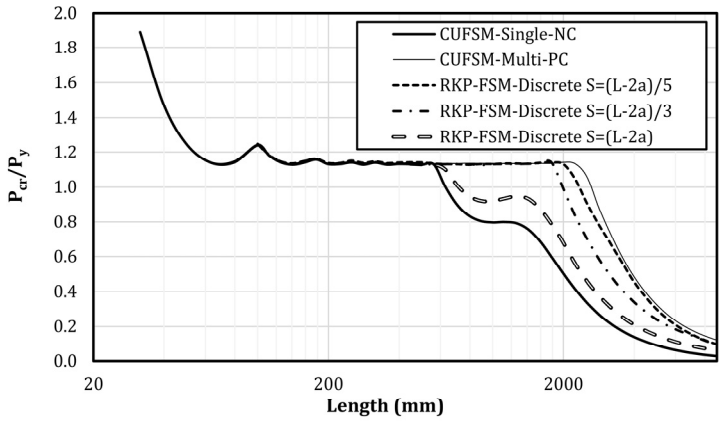

Figure 13. buckling load curves of the built-up column with multiple sections for different fastener spacing ratios

In the Table 1, a comparison is made between the buckling loads obtained for built-up members and those for non-composite sections. The table considers columns of different lengths: $L = 281.84$ mm, $L = 501.19$ mm, $L = 1000.00$ mm, and $L = 2511.59$ mm. The RKP-FSM modelling used in the presented results assumes a fastener spacing of $s = (L\text{-}2a)/5$. For members longer than 600, a substantial improvement in the buckling load factors is observed. This enhancement can be attributed to a change in the buckling mode shape resulting from the composite action between constituent sections.

Table 1. comparison of buckling loads obtained using various methods

Length	Section	CUFSM-PC (P_{cr}/Py)	Abaqus (P_{cr}/Py)	RKP-FSM (P_{cr}/Py)
	Single	1.1270	1.1658	1.1277
L = 281.84 mm	Built-up	1.1335	1.1787	1.1375
	$\%\Delta P_{cr}$	0.58%	1.11%	0.87%
	Single	1.1272	1.1307	1.1302
L = 501.19 mm	Built-up	1.1340	1.1361	1.1392
	$\%\Delta P_{cr}$	0.61%	0.48%	0.80%
	Single	0.7968	0.7853	0.7968
L = 1000.00 mm	Built-up	1.1339	1.1360	1.1303
	$\%\Delta P_{cr}$	42.31%	44.65%	41.86%
	Single	0.3375	0.3267	0.3375
L = 2511.89 mm	Built-up	1.0607	0.8318	0.8836
	$\%\Delta P_{cr}$	214.34%	154.62%	161.84%

However, the results for $L = 2511.89$ mm highlight an interesting observation. The conventionally used continuous modelling of fasteners (as with S-a FSM) can artificially yield higher buckling loads. In this case, the discrete modelling of fasteners using Abaqus and RKP-FSM produces similar loads, both of which are lower than those obtained through continuous

modelling. This emphasises the importance of the modelling approach, especially in scenarios where composite action significantly influences the buckling behaviour of longer members.

The buckling mode shapes corresponding to the lengths listed in the table are illustrated in Figure 14, Figure 15, and Figure 16. The buckling mode shapes obtained for single sections are compared with those of the built-up members, and to validate the results, the buckling mode shapes obtained using RKP-FSM are validated against those obtained using Abaqus. In Figure 14, both single and built-up sections undergo local buckling for the specific length considered (L = 281.84 mm). The mode shapes presented confirm the negligible enhancement in the buckling load, as both sections exhibit similar local buckling behaviour. Figure 15 depicts the buckling mode shapes for L = 1000.0 mm. Here, the single section undergoes distortional buckling, while the built-up column exhibits local buckling. As indicated in the table, am approximate 42% increase in the buckling load is anticipated for this length. This enhancement can be attributed to the observed change in the buckling mode shape. In Figure 16, the buckling mode shapes for L = 2511.89 mm are compared. For this length, the single section undergoes flexural global buckling, while the built-up member exhibits a flexural-torsional buckling mode shape. A significant enhancement of 154% is observed in the buckling load, aligning with the general outcomes. These mode shape comparisons provide visual confirmation of the impact of composite action on the buckling behaviour of built-up members, validating the results obtained through the RKP-FSM simulations.

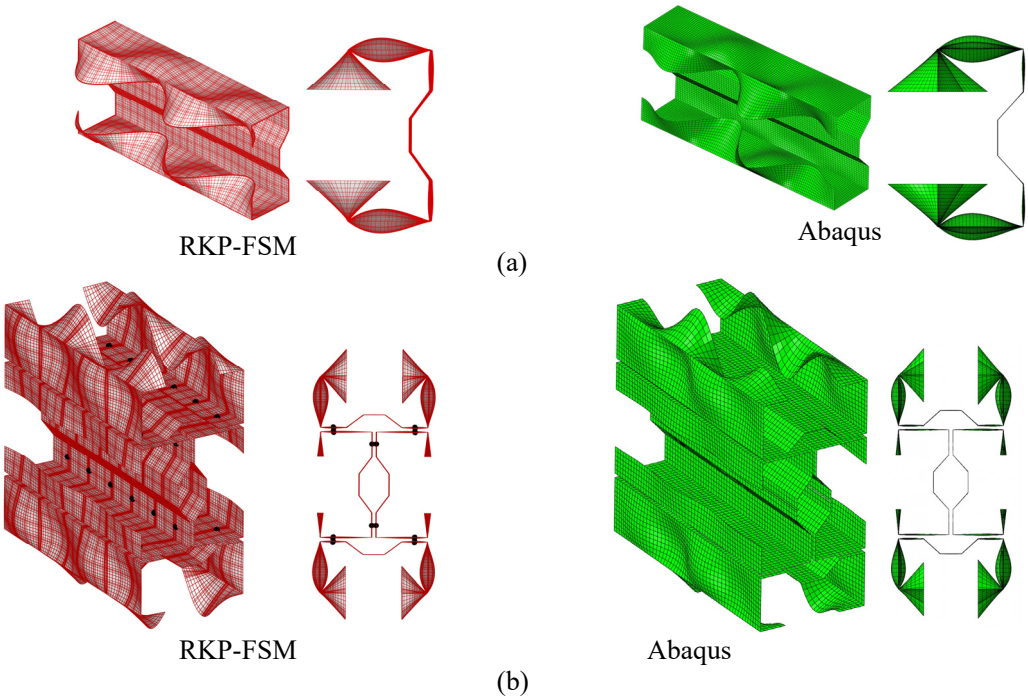

Figure 14. Comparison of buckling mode shapes of (a) single and (b) built-up sections at L = 281.84 obtained using RKP-FSM and Abaqus

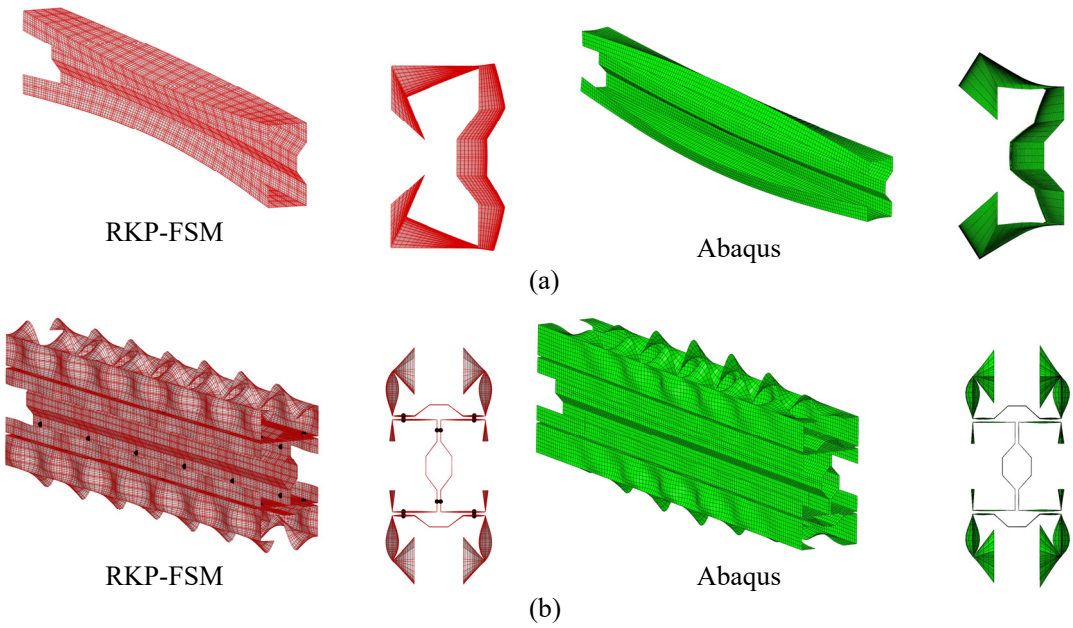

Figure 15. Comparison of buckling mode shapes of (a) single and (b) built-up sections at L = 1000.00 mm obtained using RKP-FSM and Abaqus

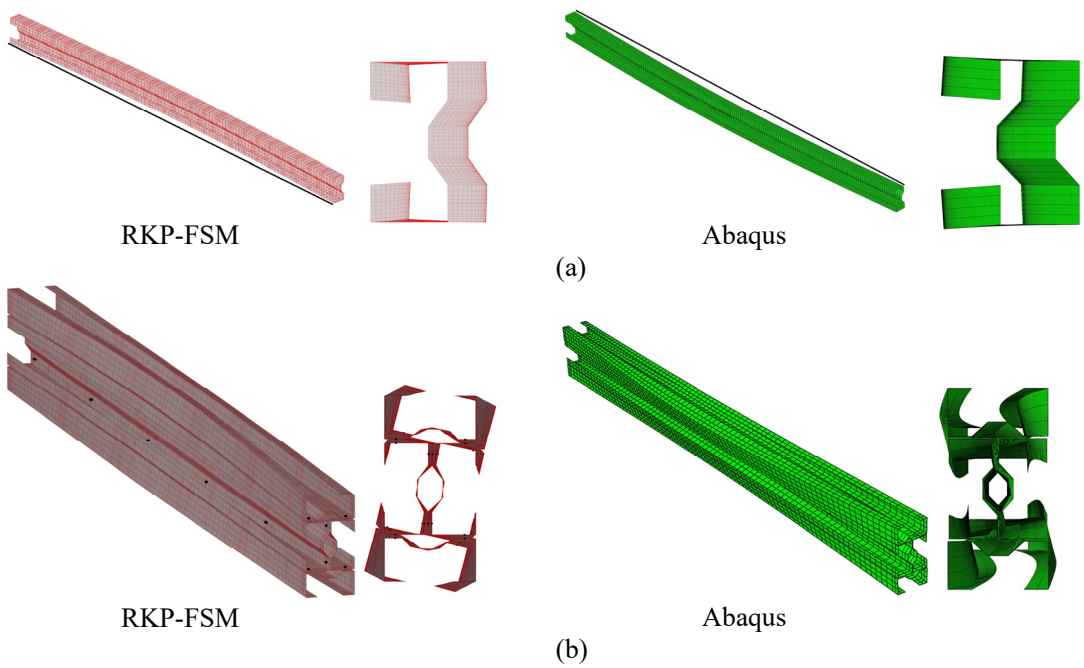

Figure 16. Comparison of buckling mode shapes of (a) single and (b) built-up sections at L = 2511.89 mm obtained using RKP-FSM and Abaqus

6 CONCLUSION

In this study, a novel and practical application of the Reproducing Kernel Particle Finite Strip Method (RKP-FSM), an extension of the finite strip method (FSM), is introduced and verified. The RKP-FSM is employed for the stability analysis of cold-formed steel (CFS) built-up sections with arbitrarily-located discrete fasteners. Numerical examples are presented to

showcase the performance and versatility of the RKP-FSM in the elastic buckling analysis of CFS built-up sections with increasingly complex geometries. The study explores the influence of fastener spacing ratios on the composite behaviour of built-up sections, revealing that reducing the spacing enhances buckling capacity, especially in the global and distortional buckling regions.

REFERENCES

[1] M. Khezri, M. Abbasi, K. Rasmussen, A combined meshfree/finite strip method for analysis of plates with perforations and cracks, Thin-Walled Structures 111 (2017) 113-125.
[2] M. Khezri, Z. Vrcelj, M. Bradford, Thin plate bending analysis and treatment of material discontinuities using the generalised RKP-FSM, Computer Modeling in Engineering & Sciences(CMES) 87(4) (2012) 271-305.
[3] S.C.W. Lau, G.J. Hancock, Buckling of thin flat-walled structures by a spline finite strip method, Thin-Walled Structures 4(4) (1986) 269-294.
[4] D.C. Fratamico, B.W. Schafer, Numerical studies on the composite action and buckling behavior of built-up cold-formed steel columns, (2014).
[5] J.-H. Zhang, B. Young, Numerical investigation and design of cold-formed steel built-up open section columns with longitudinal stiffeners, Thin-Walled Structures 89 (2015) 178-191.
[6] M. Abbasi, M. Khezri, K.J.R. Rasmussen, B.W. Schafer, Elastic buckling analysis of cold-formed steel built-up sections with discrete fasteners using the compound strip method, Thin-Walled Structures 124 (2018) 58-71.
[7] M. Abbasi, M. Khezri, K.J. Rasmussen, 07.13: On extending the direct strength method to the design of cold-formed steel built-up columns, ce/papers 1(2-3) (2017) 1600-1608.
[8] M. Khezri, M. Abbasi, K.J. Rasmussen, 07.20: Application of the compound strip method in buckling analysis of cold-formed steel built-up sections, ce/papers 1(2-3) (2017) 1667-1676.
[9] M. Khezri, Z. Vrcelj, M.A. Bradford, Thin plate bending analysis using the generalized RKP-FSM, American Environmentalism: Philosophy, History, and Public Policy 175 (2013).
[10] A. Behzadan, H.M. Shodja, M. Khezri, A unified approach to the mathematical analysis of generalized RKPM, gradient RKPM, and GMLS, Computer methods in applied mechanics and engineering 200(5-8) (2011) 540-576.
[11] H. Shodja, M. Khezri, A. Hashemian, A. Behzadan, RKPM with augmented corrected collocation method for treatment of material discontinuities, Computer Modeling in Engineering & Sciences(CMES) 62(2) (2010) 171-204.
[12] M. Khezri, M. Gharib, M. Bradford, B. Uy, A state space augmented generalised RKPM for three-dimensional analysis of thick and laminated composite plates, Computers & Structures 158 (2015) 225-239.
[13] M. Khezri, M. Gharib, M.A. Bradford, Z. Vrcelj, Analysis of thick and orthotropic rectangular laminated composite plates using a state-space-based generalised RKP-FSM, Composite Structures 133 (2015) 691-706.
[14] M. Gharib, M. Khezri, S. Foster, A. Castel, Application of the meshless generalised RKPM to the transient advection-diffusion-reaction equation, Computers & Structures 193 (2017) 172-186.
[15] M. Gharib, M. Khezri, S. Foster, Meshless and analytical solutions to the time-dependent advection-diffusion-reaction equation with variable coefficients and boundary conditions, Applied Mathematical Modelling 49 (2017) 220-242.
[16] K. Liew, G. Zou, S. Rajendran, A spline strip kernel particle method and its application to two-dimensional elasticity problems, International Journal for Numerical Methods in Engineering 57(5) (2003) 599-616.
[17] B.M. Donning, W.K. Liu, Meshless methods for shear-deformable beams and plates, Computer Methods in Applied Mechanics and Engineering 152(1–2) (1998) 47-71.
[18] W. Han, X. Meng, Error analysis of the reproducing kernel particle method, Computer Methods in Applied Mechanics and Engineering 190(46–47) (2001) 6157-6181.
[19] Z. Vrcelj, M.A. Bradford, A simple method for the inclusion of external and internal supports in the spline finite strip method (SFSM) of buckling analysis, Computers & Structures 86(6) (2008) 529-544.
[20] M. Azhari, S. Hoshdar, M.A. Bradford, On the use of bubble functions in the local buckling analysis of plate structures by the spline finite strip method, International Journal for Numerical Methods in Engineering 48(4) (2000) 583-593.
[21] M. Khezri, M.A. Bradford, Z. Vrcelj, Application of RKP-FSM in the buckling and free vibration analysis of thin plates with abrupt thickness changes and internal supports, International Journal for Numerical Methods in Engineering 104(2) (2015) 125-156.
[22] S.G. Esfahani, S. Sarrami-Foroushani, M. Azhari, On the use of reproducing kernel particle finite strip method in the static, stability and free vibration analysis of FG plates with different boundary conditions and diverse internal supports, Applied Mathematical Modelling 92 (2021) 380-409.
[23] Z. Li, B.W. Schafer, Buckling analysis of cold-formed steel members with general boundary conditions using CUFSM conventional and constrained finite strip methods, (2010).
[24] D. Systèmes, ABAQUS 2017 analysis user's guide, Dassault Systèmes (2017).